International Journal of Nanomedicine

Dovepress

open access to scientific and medical research

Open Access Full Text Article

ORIGINAL RESEARCH

Fe^{3+}@PDOPA-*b*-PSar Nanoparticles for Magnetic Resonance Imaging and Cancer Chemotherapy

Wei Sun[1,2,*], Songyi Xu[3,*], Tianlun Shen[1,3,*], Guangyao Li[1], Jingfeng Zhang[2], Chunshu Pan[1,2], Wei Lu[1,2], Xiangrui Liu[1], Jianjun Zheng[2], Jun Ling[1,3], Jihong Sun[1]

[1]Department of Radiology, Sir Run Run Shaw Hospital, Zhejiang University School of Medicine, Hangzhou, People's Republic of China; [2]Department of Radiology, Ningbo No. 2 Hospital, Ningbo, People's Republic of China; [3]MOE Key Laboratory of Macromolecular Synthesis and Functionalization, Department of Polymer Science and Engineering, Zhejiang University, Hangzhou, People's Republic of China

*These authors contributed equally to this work

Correspondence: Jihong Sun, Department of Radiology, Sir Run Run Shaw Hospital, Zhejiang University School of Medicine, Tel +86 13857176538, Email sunjihong@zju.edu.cn; Jianjun Zheng, President of Ningbo No. 2 Hospital, Ningbo, People's Republic of China, Tel +86 574 83870280, Email zhjjnb2@163.com

Purpose: Chemotherapy treatments for cancer are always accompanied by a low concentration of drug delivered in the tumor area and severe side effects including systemic toxicity. Improving the concentration, biocompatibility, and biodegradability of regional chemotherapy drugs is a pressing challenge in the field of materials.

Methods: *N*-Phenyloxycarbonyl-amino acids (NPCs) which exhibit significant tolerance to nucleophiles, such as water and hydroxyl-containing compounds, are promising monomers for the synthesis of polypeptides and polypeptoids. Cell line and mouse models were used to comprehensively explore how to enhance the tumor MRI signal and evaluate the therapeutic effect of Fe@POS-DOX nanoparticles.

Results: In this study, poly(3,4-dihydroxy-L-phenylalanine)-*b*-polysarcosine (PDOPA-*b*-PSar, simplified as POS) was synthesized by the block copolymerization of DOPA-NPC with Sar-NPC. Fe@POS-DOX nanoparticles were prepared in order to utilize the strong chelation of catechol ligands to iron (III) cations and the hydrophobic interaction between DOX and DOPA block to deliver chemotherapeutics to tumor tissue. The Fe@POS-DOX nanoparticles exhibit high longitudinal relaxivity (r_1 = 7.06 $mM^{-1}{\cdot}s^{-1}$) and act as T_1-weighted magnetic resonance (MR) imaging contrast agents. Further, the main focus was improving tumor site-specific bioavailability and achieving therapeutic effects through the biocompatibility and biodegradability of Fe@POS-DOX NPs. The Fe@POS-DOX treatment exhibited excellent antitumor effects.

Conclusion: Upon intravenous injection, Fe@POS-DOX delivers DOX specifically to the tumor tissues, as revealed by MR, and leads to the inhibition of tumor growth without overt toxicity to normal tissues, thus displaying considerable potential for use in clinical applications.

Keywords: poly (α-amino acid)s, polypeptides, polypeptoids, MRI, chemotherapy, nanoparticles

Introduction

Chemotherapy is among the main clinical treatments for cancer, and can have remarkable results.[1] However, the clinical side effects of chemotherapy are reflected in the low concentrations of drug delivery at the tumor area and serious systemic toxicity, which can lead to tumor recurrence and metastases.[2–6] Chemotherapeutic drug delivery has benefitted from nanotechnology and achieved an effective anti-cancer strategy through the enhanced permeability and retention (EPR) effect,[7,8] which improves the retention time and the accumulation of particles at the tumor site through passive targeting techniques.[9] This not only enhances therapeutic efficacy, but also reduces normal tissues damage. However, nanoplatforms are considerably limited by the degradation, metabolism, and long-term toxicity of nanomaterials in the body,[10,11] which is a key challenge for their future clinical applications.[12]

Received: 28 October 2022
Accepted: 11 April 2023
Published: 26 April 2023

Graphical Abstract

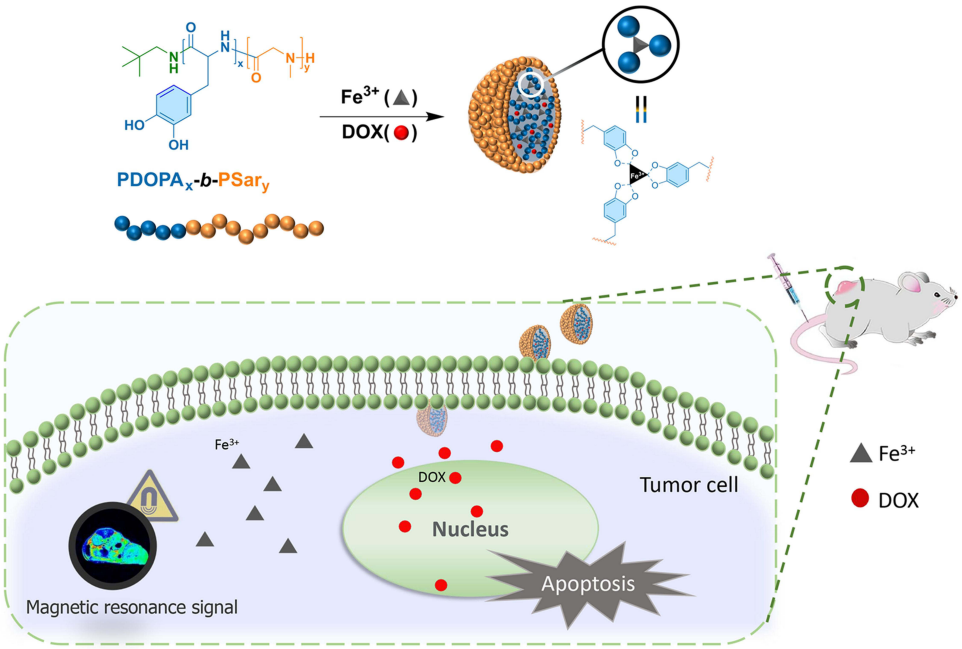

Poly(α-amino acid)s (PAAs), including polypeptides and polypeptoids, exhibit inherent biocompatibility and biodegradability, which negate concerns about their potential long-term toxicity. They are widely applied across several biomedical fields, including controlled drug release, gene delivery, stimuli-responsive biomaterials, and nanoscale self-assembly systems.[13–18] In addition to previous work on diblock copolymerization synthesized with NTA monomers,[19] our group has utilized the *N*-phenoxycarbonyl α-amino acid (NPC) approach. This approach benefits from excellent tolerance to hydroxyl groups in primary amine-mediated polymerization. Fe^{3+}, a paramagnetic metal and a necessary trace element for the human body, has low biotoxicity.[20] Moreover, Fe^{3+} with five unpaired electrons has a high longitudinal relaxivity for magnetic resonance imaging (MRI).[21]

In this study, Fe^{3+}@PDOPA-*b*-PSar nanoparticles loaded with the chemotherapy drug doxorubicin (DOX) (labeled as Fe@POS-DOX NPs) were developed with a suitable size and degradability to enhance the accumulation and penetration depth of particles at the tumor site. Fe@POS-DOX NPs respond to tumor microenvironment and release DOX and Fe^{3+}, which act in concert to produce optimal therapeutic effects and function as a contrast for MRI imaging. The biological activity and imaging performance were evaluated through in vitro and in vivo experiments. Fe@POS-DOX NPs have significant potential for applications as drug delivery systems and bioimaging contrast agents.[22,23]

Materials and Methods

Materials

Phenyl chloroformate (PCF), sarcosine, 3,4-dihydroxy-$_L$-phenylalanine ($_L$-DOPA), hexafluoroisopropanol (HFIP), neopentylamine (NPA), *N,N*-diisopropylethylamine (DiPEA), potassium trifluoroacetate (CF_3COOK), fluorescein isothiocyanate isomer I (FITC), dimethylacetamide (DMAc, super dry, sealed under argon), and deuterated dimethyl sulfoxide (DMSO-d_6) were purchased from the Shanghai Energy Chemicals Co, Ltd. (Shanghai, China). Dimethyl sulfoxide (DMSO), ferric nitrate nonahydrate ($Fe(NO_3)_3{\cdot}9H_2O$), diethyl ether, ethyl acetate (EA), petroleum ether (PE) and sodium ethoxide (EtONa) were purchased from the Sinopharm Chemical Reagent Co. Ltd. (Shanghai, China). Doxorubicin

hydrochloride (DOX·HCl) was purchased from BBI Co. Ltd. (Shanghai, China). The NPA was stirred over CaH_2, followed by distillation under reduced pressure. Other materials were used as received.

Characterization

Nuclear magnetic resonance (NMR) spectra were recorded using a Bruker Avance DMX 400 spectrometer (^{1}H: 400 MHz). The size exclusion chromatography (SEC) instrument consisted of a Waters 1515 isocratic HPLC pump, Waters 2414 interferometric refractometer (RI), and two Shodex KF series columns. Hexafluoroisopropanol containing 3 mg/mL of potassium trifluoroacetate was used as the eluent at a flow rate of 0.8 mL/min at 40 °C. Commercial poly(methyl methacrylate) standards with narrow dispersities were used for molecular weight (MW) calibration. The Fe^{3+} concentrations were determined by inductively coupled plasma mass spectrometry (ICP-MS) using a Thermo XSeries II spectrometer (Thermo Fisher Scientific, USA). An ultraviolet-visible (UV-vis) spectrophotometer (Molecular Devices SpecteaMax M5e, USA) was used to analyze the absorption spectra of the NPs during fabrication in a quartz cuvette. A particle size analyzer (Zetasizer Nano Series, Malvern Instruments) was used to evaluate size distributions. A JEM-1400plus electron microscope with an accelerating voltage of 120 kV was used for transmission electron microscopy (TEM) imaging to detect the morphology of the NPs. Uranyl acetate (4 wt.%) was used to stain the samples before TEM imaging.

Preparation of Fe@POS-DOX NPs

Synthesis of *N*-Phenyloxycarbonyl-Sarcosine (Sar-NPC) and *N*-Phenyloxycarbonyl-3,4-Dihydroxy-$_L$-Phenylalanine ($_L$-DOPA-NPC)

Sarcosine (22.27 g, 0.25 mol) and PCF (31.1 mL, 0.25 mol) were suspended in 250 mL of EA. The mixture was heated to 45 °C and maintained at this temperature for 48 h. Next, unreacted sarcosine was removed via filtration. After evaporation of EA under reduced pressure, the crude product was purified by column chromatography (gradient eluent EA:PE = 1:5–1:1) to obtain Sar-NPC in the form of a light-yellow viscous liquid (11.67 g, yield: 22.5%). ^{1}H NMR (DMSO-d_6) δ: 3.01 (d, 3H, J = 58.8 Hz), 4.07 (d, 2H, J = 50.4 Hz), 7.00–7.47 (m, 5H), 12.90 (s, 1H).

$_L$-DOPA (29.56 g, 0.15 mol) and PCF (19.1 mL, 0.15 mol) reacted following the same procedure above, thereby producing $_L$-DOPA-NPC in the form of a white powder (8.35 g, yield: 17.4%). ^{1}H NMR (DMSO-d_6) δ: 2.66–2.98 (m, 2H), 4.10 (m, 1H), 6.51–7.40 (m, 8H), 8.06 (d, 1H, J = 8.40 Hz), 8.67–8.85 (m, 2H), 12.79 (s, 1H).

Diblock Copolymerization of $_L$-DOPA-NPC with Sar-NPC

Diblock copolymerization was performed in pre-dried and argon-purged vials using the Schlenk technique. $_L$-DOPA-NPC (0.4050 g, 1.276 mmol) was added to a vial and dissolved in 1.30 mL of dry DMAc. Subsequently, 1.27 mL of NPA in DMAc solution (0.0956 mol/L) was added to the solution using a syringe. The vial was sealed and heated to 60 °C and maintained at that temperature for 24 h to form the first block solution. Next, Sar-NPC (3.016 g, 14.42 mmol) and DiPEA (0.3044 g, 2.336 mmol) were dissolved in 28.0 mL of dry DMAc. Subsequently, 2.00 mL of the first block solution was added using a syringe. The vial was sealed and heated to 60 °C and maintained for 48 h. The diblock copolymer was precipitated from diethyl ether, collected via centrifugation, and dried under vacuum conditions (POS, 0.598 g, yield: 50%).

Preparation of Fe@POS-DOX NPs

NPs were prepared in pre-dried and argon-purged vials using the Schlenk technique. POS (77.6 mg, 0.077 mmol of DOPA units) was dissolved in 1.0 mL of DMSO. Next, 1.0 mL DMSO solution of DOX (16.1 mg DOX·HCl, 0.028 mmol, neutralized by EtONa), 1.0 mL DMSO solution of EtONa (5.2 mg, 0.077 mmol) and 1.0 mL DMSO solution of Fe $(NO_3)_3 \cdot 9H_2O$ (32.7 mg, 0.081 mmol) were added by syringe under continuous stirring. After 30 min, deionized water (10 mL after argon bubbling to remove oxygen) was slowly added to the solution using a syringe pump (Perfusor Compact) over 3 h. The mixture was dialyzed against deionized water for 24 h by changing the dialysis medium every 8 h to remove any impurities. DOX-loaded Fe^{3+}@PDOPA-*b*-PSar nanoparticles were concentrated using ultrafiltration centrifugal technology. When the concentration of POS in Fe@POS-DOX was 1.0 mg/mL, the concentration of Fe^{3+} was found to be 18.0 μg/mL according to ICP-MS analysis.

Preparation of DOX Loaded Fe^{3+}@PDOPA-b-PSar NPs Labeled with IRDye800CW

NPs were prepared in pre-dried and argon-purged vials using the Schlenk technique. All the vials were kept in the dark. POS (74.3 mg, 0.074 mmol of DOPA unit) and IRDye800CW NHS ester (0.5 mg, 0.00043 mmol) were dissolved in DMSO (1.0 mL). After 24 h, 1.0 mL DMSO solution of DOX (7.2 mg DOX·HCl, 0.012 mmol, neutralized by EtONa), 1.0 mL DMSO solution of EtONa (5.0 mg, 0.074 mmol) and 1.0 mL DMSO solution of $Fe(NO_3)_3{\cdot}9H_2O$ (30.6 mg, 0.076 mmol) were added by syringe under continuous stirring. After 30 min, deionized water (10 mL, after argon bubbling to remove oxygen) was slowly added to the solution using a syringe pump for 3 h. The mixture was dialyzed against deionized water for 24 h by changing the dialysis medium every 8 h to remove any impurities. DOX-loaded Fe^{3+}@PDOPA-b-PSar NPs labeled with IRDye800CW (labeled as Fe@POS-DOX-IRDye800CW) were concentrated using ultrafiltration centrifugal technology. When the concentration of POS in Fe@POS-DOX-IRDye800CW was 1.0 mg/mL, the concentration of Fe^{3+} was found to be 17.3 μg/mL according to ICP-MS analysis.

Preparation of DOX Loaded Fe^{3+}@PDOPA-*b*-PSar NPs Labeled with FITC

NPs were prepared in pre-dried and argon-purged vials using the Schlenk technique. All the vials were kept in the dark. POS (65.3 mg, 0.065 mmol DOPA unit) and FITC (2.1 mg, 0.0054 mmol) were dissolved in DMSO (1.0 mL). After 24 h, 1.0 mL DMSO solution of DOX (6.1 mg DOX·HCl, 0.011 mmol, neutralized by EtONa), 1.0 mL DMSO solution of EtONa (4.4 mg, 0.065 mmol) and 1.0 mL DMSO solution of $Fe(NO_3)_3{\cdot}9H_2O$ (29.7 mg, 0.073 mmol) were added by syringe with continuous stirring. After 30 min, deionized water (10 mL after argon bubbling to remove oxygen) was slowly added to the solution using a syringe pump for 3 h. The mixture was dialyzed against deionized water for 24 h by changing the dialysis medium every 8 h to remove any impurities. DOX-loaded Fe^{3+}@PDOPA-b-PSar NPs labeled with FITC (labeled as Fe@POS-DOX-FITC) were concentrated using ultrafiltration centrifugal technology. When the concentration of POS in Fe@POS-DOX-FITC was 1.0 mg/mL, the concentration of Fe^{3+} was found to be 14.3 μg/mL according to ICP-MS analysis.

DOX Release from Fe@POS-DOX NPs

Drug release experiments were conducted in a simulated acidic tumor microenvironment (phosphate-buffered saline, PBS solution with a pH of 5.5). The determined amount of Fe@POS-DOX NPs (containing 2 mg DOX) was dispersed in 5 mL of PBS solution with a pH of 5.5, and then transferred into a dialysis bag (cutoff MW: 10 kg/mol) placed in 50 mL of the previously mentioned media. The sample was stirred at 60 rpm at 37 °C. Next, 1.0 mL of the sample was collected at predetermined time intervals, and an equal amount of the same medium was added. The drug content of each sample was measured using ultraviolet absorption spectroscopy.

Cell Culture and Tumor Model Establishment

Mouse breast 4T1-fluc tumor cells (American Tissue Type Culture Collection, Manassas, VA, USA) were cultured in RPMI 1640 medium (Life Technologies) containing 10% fetal calf serum (Life Technologies) in a humidified incubator with 5% CO_2 and 95% air at 37 °C. BALB/c mice (female, 6-week-old, 20 g) were purchased from Zhejiang Vital River Laboratory Animal Technology Co. Ltd. All procedures were performed in accordance with guidelines approved by the Institutional Animal Care and Use Committee. BALB/c orthotopic tumor implantation was established by injecting groin of the right hindlimb of each mouse with 1×10^6 4T1-fluc cells in 200 μL PBS. When the tumor volume was 100 mm^3, 6 d after implantation, the mice were subsequently used for imaging and therapeutic experiments.

MRI in vivo

The mice were injected with Fe@POS-DOX NPs, and the biodistribution of the nanoparticles was examined using MRI (GE Signa HDxt 3.0 Tesla). All images were acquired using the following parameters: repetition time/echo time = 400/15 ms, 512×512 matrices, slices = 5, thickness = 2 mm, averages = 12, FOV = 90×90. Transverse images of the tumor-bearing mice were dynamically acquired from 0 to 12 h post-intravenous injection (200 μL of Fe@POS-DOX solution, 2.0 mg/kg). The MRI signal intensity of the tumor-to-background ratio (TBR) was analyzed quantitatively. The equation of TBR is as follows:

$$\text{TBR} = \frac{\text{Average MRI intensity of the tumor area}}{\text{Average MRI intensity of the background area}}$$

Fluorescence Imaging (FI) ex vivo

The mice were injected with Fe@POS-DOX NPs and euthanized 24 h post-injection. Tumors and major organs (hearts, livers, spleens, lungs, kidneys) were dissected for ex vivo FI. Fe@POS-DOX NPs were also identified for quantitative analysis with optical IVIS (In Vivo Imaging Systems) Living Imaging software (version 3.0, PerkinElmer, USA).

Bioluminescence Imaging (BLI) in vivo and ex vivo

An optical IVIS was used to assess the therapeutic effects in the 4T1 breast cancer model. The mice were anesthetized with tribromoethanol and tertiary amyl alcohol, and were injected with 100 μL D-luciferin (40 mg/mL), via intraperitoneal injection 5 min before BLI. The BLI intensity of the tumor was dynamically measured and analyzed every 5 d using IVIS Living Image software. Tumor volume and body weight were monitored and recorded to evaluate treatment efficacy.

Statistics

Statistical analysis was performed utilized GraphPad Prism V8.0 (GraphPad Software, Inc., San Diego, CA, USA). To analyze differences within and between groups, one-way ANOVA with Tukey's multiple comparisons test or Student's *t*-test were used. All data are expressed as *mean ± standard error of the mean* (SEM). Values of *P < 0.05, **P < 0.01, and ***P < 0.001 were considered statistically significant.

Results and Discussion

Preparation and Characterization of Fe@POS-DOX

The diblock copolymer PDOPA-*b*-PSar (POS) was synthesized via sequential polymerizations of Sar-NPC (Figure S1) and $_{L}$-DOPA-NPC (Figure S2) initiated by NPA. The ^{1}H NMR spectrum of POS (Figure 1A) illustrates the complete assignment of the proton signals of the DOPA and sarcosine units. The signal of methyl protons in sarcosine units (H^{k}) appears in the broad range of 2.59–3.04 ppm. The characteristic signals of the DOPA unit in the ranges of 8.59–8.88 ppm ($H^{m,\ n}$), 7.63–8.05 ppm (H^{e}), and 6.27–6.77 ppm ($H^{g,\ h,\ i}$) were attributed to the phenolic hydroxyl, amide, and aromatic protons, respectively. The methylene proton signals on the backbone of the sarcosine unit (H^{j}) overlap with those of methyne protons on the backbone of the DOPA unit (H^{d}) between 3.68 and 4.57 ppm. The composition of the copolymer ($PDOPA_{10}$-*b*-$PSar_{117}$) and the molecular weights (10.2 kg/mol) were calculated according to the intensities of *tert*-butyl group protons (H^{a}) and the characteristic signals of H^{k} and $H^{g,\ h,\ i}$. The SEC traces (Figure 1B) indicate that the retention time of POS decreased from the first block (PDOPA), which suggests that all terminal amine groups of PDOPA successfully initiate the polymerization of Sar-NPC. Fe@POS-DOX NPs were prepared using the solvent exchange method with 1.5–2% Fe content and 7.5–9% DOX content, as described in the Experimental section.

The hydrodynamic diameters and size distributions were characterized using dynamic light scattering (DLS). As shown in Figure 1C, Fe@POS-DOX NPs exhibited a narrow dispersity with a hydrodynamic diameter of 16.5 nm. The Fe@POS-DOX NPs remained unchanged in size over 10 d and did not exhibit an aggregation tendency (Figure 1D), showing very high overall stability. Their size and morphologies were characterized by TEM and the Fe@POS-DOX NPs were found to be spherical with a homogeneous size distribution of approximately 20 nm (Figure 1E).

To investigate the DOX release behavior, the amount of DOX released from Fe@POS-DOX NPs at a pH of 5.5 was calculated. As shown in Figure 1F, approximately 80% of DOX was released within 48 h, obviously higher than that pH 7.4 control group (approximately 50%). This was expected because the strong Fe^{3+}-DOPA chelation would be significantly disrupted at a pH of 5.5,[24] which represented a simulated cancer cell environment. This phenomenon ensured the success of the pH-regulated drug release, thereby facilitating the therapeutic effect of Fe@POS-DOX NPs in the simulated tumor microenvironment.

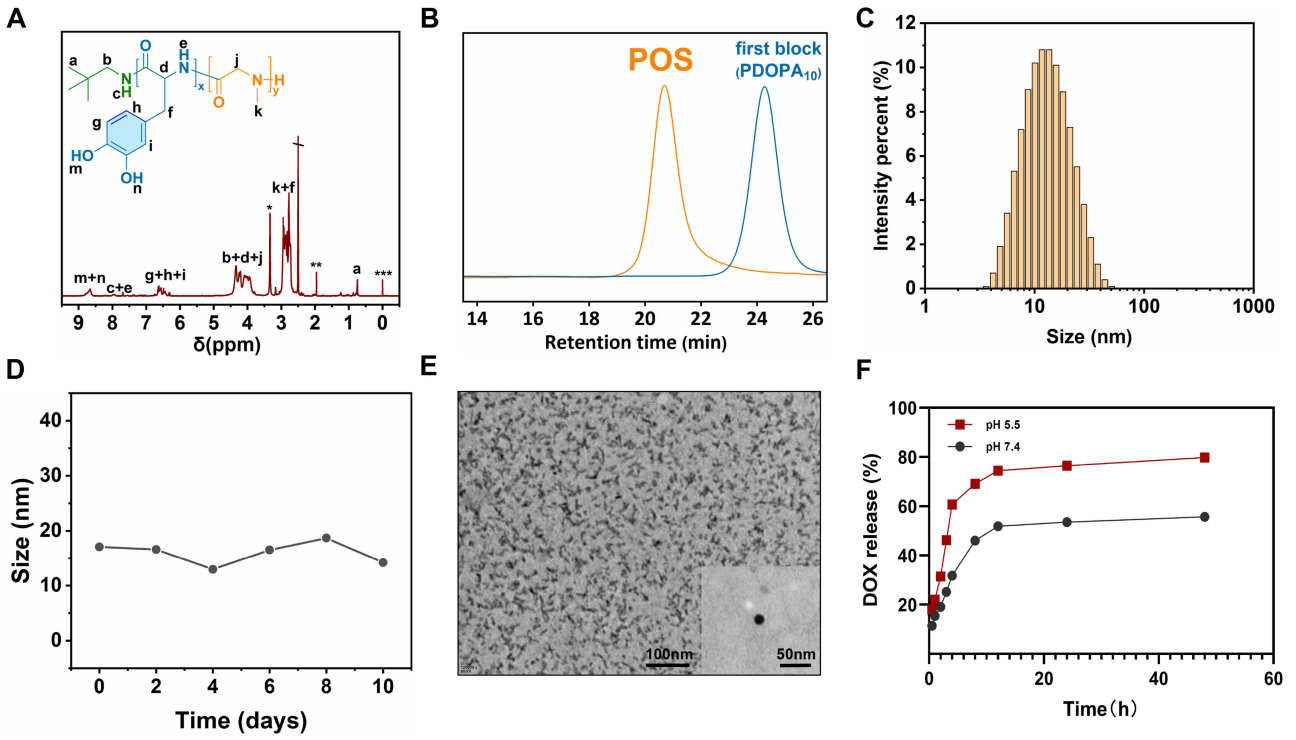

Figure 1 (**A**) ^{1}H NMR spectrum of POS in DMSO-d_6 (* H_2O, ** DMAc, *** TMS, / DMSO). Polymer composition is determined as $PDOPA_{10}$-*b*-$PSar_{117}$. (**B**) SEC traces of POS ($M_{n\ SEC}$ = 28.1 kg/mol, $Đ$ = 1.12) and $PDOPA_{10}$ ($M_{n\ SEC}$ = 4.0 kg/mol, $Đ$ = 1.14) after the protection of the hydroxyl groups of PDOPA by acetic anhydride. (**C**) DLS spectrum of Fe@POS-DOX in deionized water at 25 °C. (**D**) The size change of Fe@POS-DOX within 10 days. (**E**) TEM image of Fe@POS-DOX NPs. The scale bar is 50nm and 100 nm. (**F**) Release profile of DOX at pH of 7.4 and 5.5.

Furthermore, we aimed to identify possible underlying therapeutic effects in vitro. An in vitro 4T1 murine breast cancer cell viability assay was completed to assess the potential cytotoxicity of Fe@POS-DOX NPs. The cytotoxicity of Fe@POS-DOX NPs against tumor cell lines was quantified by the Cell Counting Kit-8 (CCK-8) assay. The Fe@POS-DOX NPs and free DOX (the same dose of DOX) showed significant concentration-dependent cytotoxicity. The maximum concentration of Fe@POS-DOX NPs was 1000 μg/mL (Figure 2A).

An Annexin V-FITC/PI double staining kit (Meilunbio, Dalian, China) was used for the apoptosis experiment of tumor cells in vitro, and the apoptotic rates of different treatment groups were measured by flow cytometry (CytoFLEX LX, Beckman Coulter, USA). The data revealed significantly ($P<0.01$) increased apoptosis rates in the Fe@POS-DOX group (22.83 ± 2.12%) and free DOX group (22.29 ± 3.62%) compared to that of the control group (12.28 ± 2.00%) (Figure 2B-E). Fe@POS-DOX efficiently promoted apoptosis in tumor cells.

The in vivo Bio-Distribution of Fe@POS-DOX Using MRI

The T_1-weighted MRI of Fe@POS-DOX was performed at 20 °C. Fe@POS-DOX samples were diluted in PBS with different Fe concentrations (0.20, 0.40, 0.60, 0.80 and 1.0 mM). The longitudinal relaxivity (r_1) of Fe@POS-DOX was 7.06 $mM^{-1}\cdot s^{-1}$, as shown in Figures 3A and B, which is significantly higher than that of Gd-DOTA (3.30 ± 0.25 $mM^{-1}\cdot s^{-1}$).[25]

The in vivo MRI ability of the Fe@POS-DOX NPs was studied in a mouse 4T1 breast tumor model (n = 3) at pre-, 0, 1, 2, 4, 8, and 12 h after the injection of NPs. As shown in Figure 3C, before the injection of Fe@POS-DOX NPs, only the tumor anatomic structure could be observed, with no signal from the nanoparticle. After the injection of Fe@POS-DOX NPs, more MRI signals were detected inside the tumors over the monitoring time. These signals gradually increased between 0 and 4 h post-injection and slightly decreased 8 h post-injection, thus suggesting an appreciable tumor penetration by the Fe@POS-DOX NPs. The MRI-TBR was quantified and the results are shown in Figure 3D. Evidently, the Fe@POS-DOX NP delivery based on the EPR effect had a much longer retention time and lower excretion

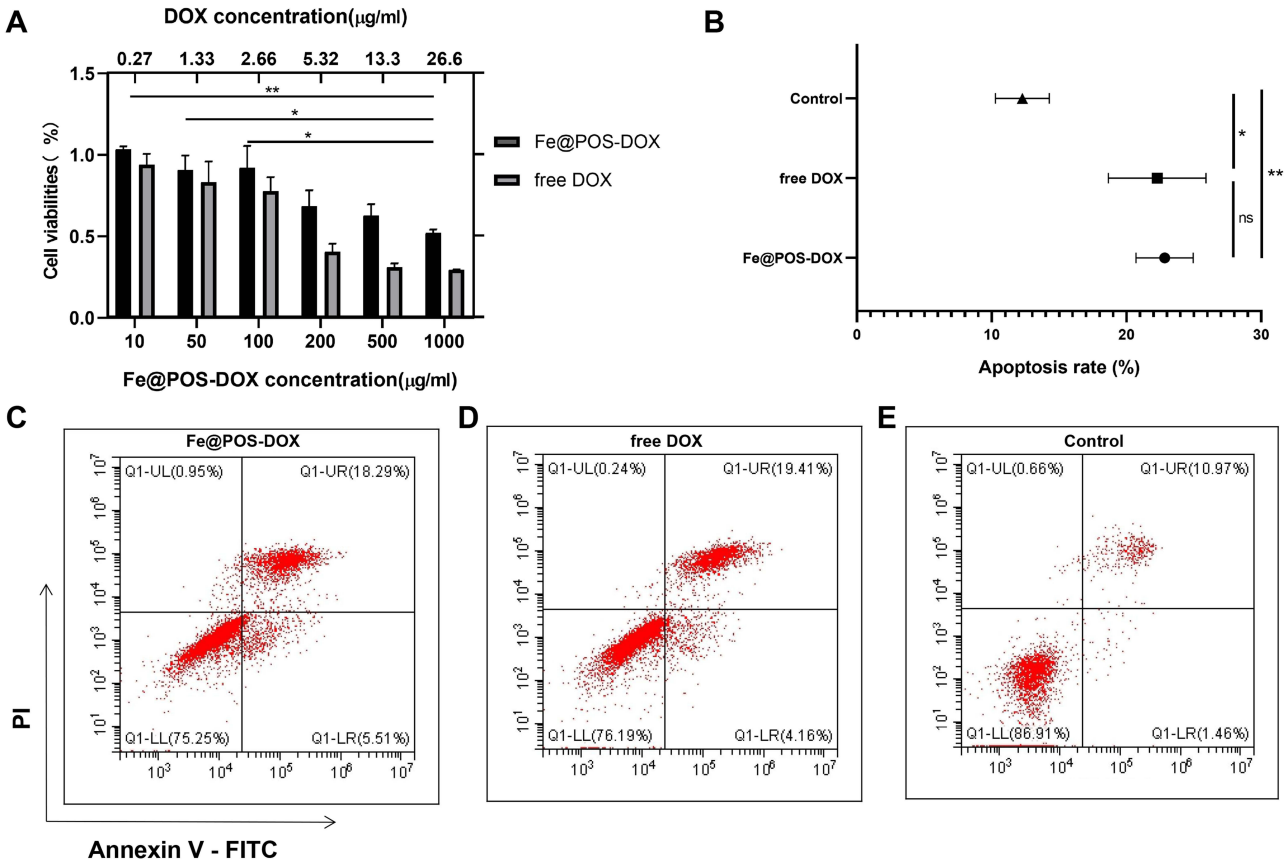

Figure 2 (**A**) The concentration-dependent cell viability profiles for Fe@POS-DOX and free DOX. The doses of DOX in every group of Fe@POS-DOX and free DOX are identical. (**B**) Quantification of apoptotic rate in the Fe@POS-DOX group, the free DOX group and the control group. (**C**) The apoptotic rate of 4T1 breast cancer cells with Fe@POS-DOX. (**D**) The apoptotic rate of 4T1 breast cancer cells with free DOX. (**E**) The apoptotic rate of 4T1 breast cancer cells in the control group. Values are expressed as the mean ± standard deviation (n=3). **P<0.01 *P<0.05.
Abbreviations: PI, propidium iodide; Q, quadrant.

rate in tumors than Gd complex small molecules.[26] This considerably improves tumor-selective imaging and further therapeutic effects in tumors.

The ex vivo Bio-Distribution of Fe@POS-DOX Using FI

FI is typically used to detect nanoparticles, with inherent advantages including higher specificity and sensitivity. Herein, 4T1 breast tumor-bearing mice (n = 3) were injected with Fe@POS-DOX-IRDye800CW via the tail vein. Ex vivo fluorescence imaging 24 h after injection outlined the distribution of Fe@POS-DOX-IRDye800CW in tumors and different organs (Figure 3E). The tumor, liver, and kidney exhibited much higher fluorescence intensity compared with that in the other organs, which indicated that Fe@POS-DOX-IRDye800CW was concentrated in the tumor region and metabolized through the liver and kidney. The fluorescence intensities of the tumors and major organs are shown in Figure 3F. Moreover, to further determine the quantitative distribution of Fe@POS-DOX, the tumors and main organs were collected 24 h after the injection of Fe@POS-DOX and the fluorescence signal emitted by the DOX in the NPs was measured using a microplate reader. The data revealed that the distribution of the DOX content in tumors and organs (Figure 3G) was consistent with the ex vivo fluorescence imaging data.

In vivo Chemotherapy

Mice with 4T1 breast tumors were treated with Fe@POS-DOX NPs (Figure 4A). Herein, 24 mice were randomly divided into four groups and underwent different treatments (six mice in each group). This included PBS, Fe@POS NP, free

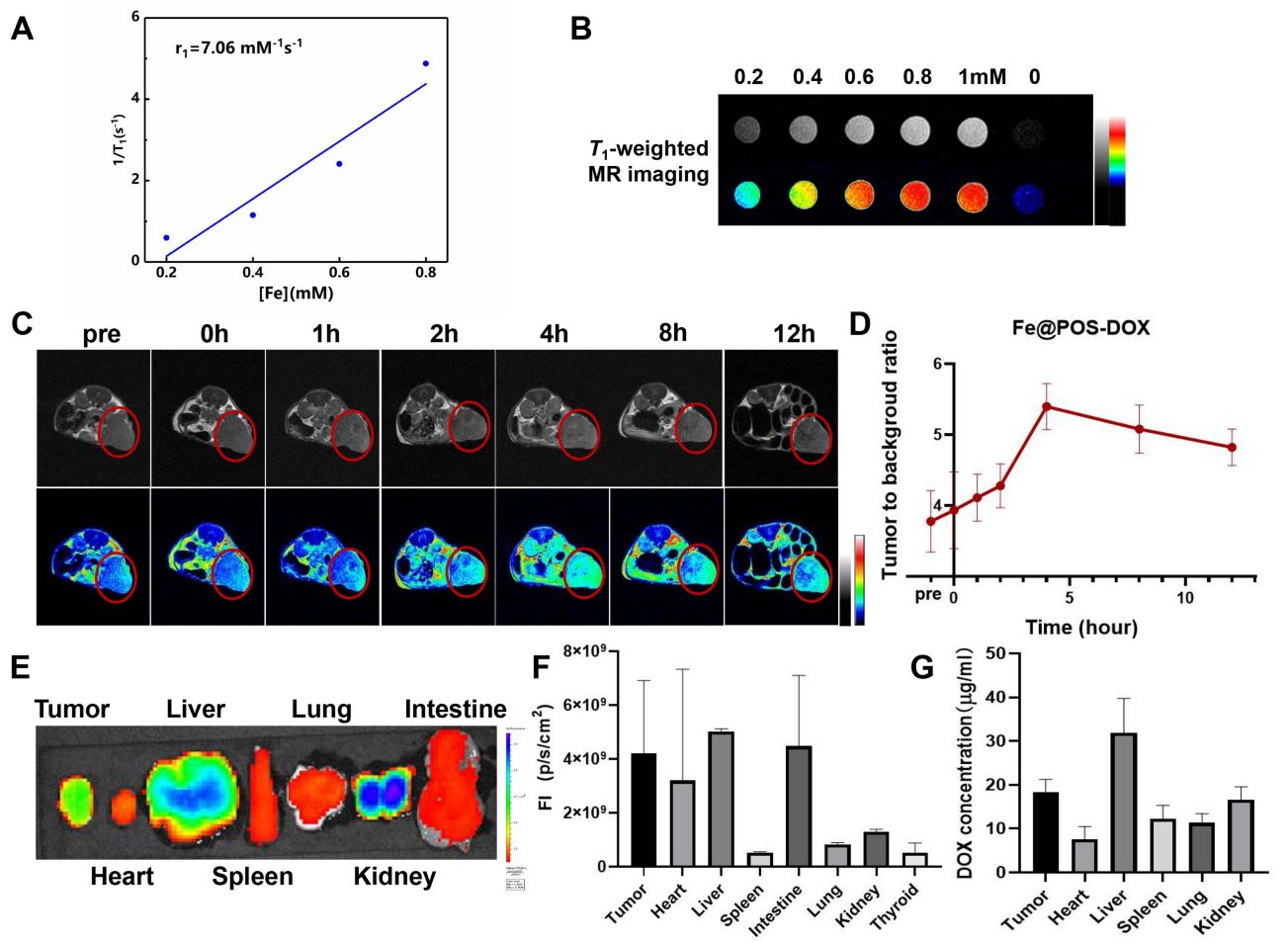

Figure 3 MRI and FI of the bio-distribution and tumor targeting effects of Fe@POS-DOX in 4T1 tumor-bearing mice. (**A**) T_1 relaxation rates of Fe@POS-DOX at a magnetic field of 3.0 T. (**B**) T_1-weighted images of Fe@POS-DOX at different Fe concentrations on a 3.0 T MRI scanner. (**C**) Plot of the MRI of Fe@POS-DOX in tumors at different time points (n = 3). (**D**) TBR of MRI signal at different time points. (**E**) Ex vivo FI for tumor and major organs at 24 h post-injection. (**F**) Mean FI intensity of tumor and major organs at 24 h post-injection. (**G**) Quantitative measurement of DOX concentration in tumor and major organs at 24 h post-injection.

DOX, and Fe@POS-DOX NP injections. The injectable Fe@POS-DOX NP solution included 10 mg/kg DOX, and 150 μL Fe@POS-DOX NPs were intravenously injected on days 6, 9, and 12 after tumor inoculation (day 0). The BLI signal intensity of the mice was dynamically monitored to assess the therapeutic effects on orthotopic 4T1 tumors in vivo for 21 continuous days (Figure 4B), and the BLI intensity was further analyzed (Figure 4C). The BLI signals of the tumors in the PBS and Fe@POS NP groups continued to increase with rapid tumor growth. The BLI signal from the tumors treated with only free DOX increased relatively slowly owing to free DOX chemotherapy. Nanoparticle-based chemotherapeutic drug delivery platforms have emerged as efficient tools to overcome the systemic toxicity associated with traditional formulations.[27]

In this study, the main focus was improving tumor site-specific bioavailability and achieving therapeutic effects through the biocompatibility and biodegradability of Fe@POS-DOX NPs. The Fe@POS-DOX treatment group exhibited excellent antitumor effects. Tumor volume was also dynamically monitored (Figure 4D), and calculated according to the formula

$$\text{Tumor volume} = \frac{\text{width}^2 \text{ x length}}{2}$$

The results were in agreement with the BLI data in vivo (Figures 4E and F). This study achieved a better therapeutic effect compared with the free DOX. The same dose of chemotherapy agent can reduce the number of treatments and improve the therapeutic effects.

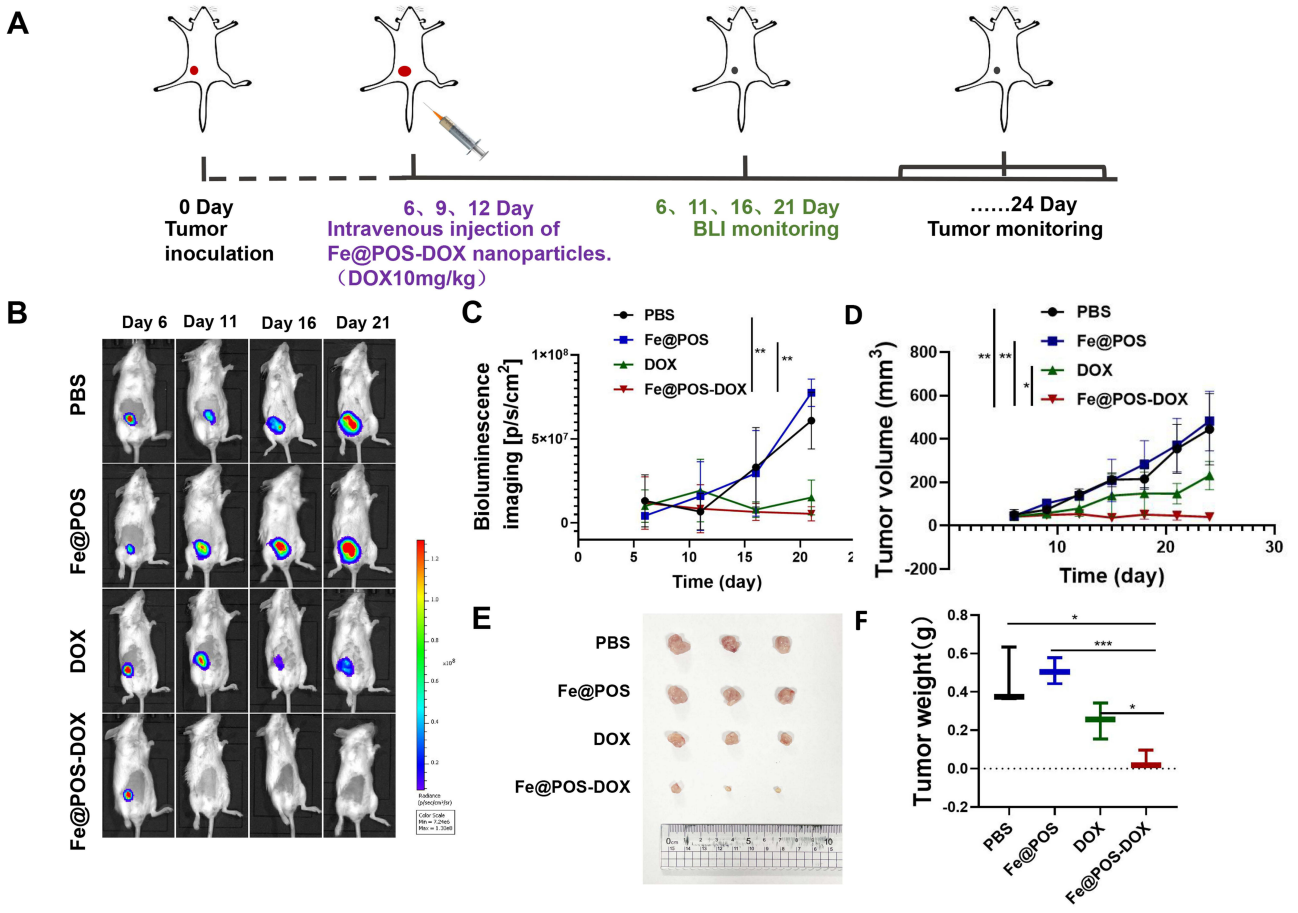

Figure 4 Evaluation of therapeutic effects with different treatments (n = 6). (**A**) Scheme showing the experimental design to evaluate the therapeutic effect. (**B**) The dynamic BLI images of 4T1 tumor bearing mice with different treatments during 21 days. (**C**) Quantification of the BLI signal of tumors after different treatments. (**D**) Tumor volume measurement for different treatment groups. (**E** and **F**) Photographs and weights of excised tumors at the end point for different treatment groups.

No obvious weight loss was observed in the different treatment groups of mice, except in the free DOX and Fe@POS-DOX NP treatment groups during the treatment period (Figure 5A). The toxicity of the nanoparticles was further analyzed. The toxicity of Fe@POS-DOX NP-based chemotherapy was examined, and liver damage was assessed using serum hepatotoxicity markers, including aspartate aminotransferase (AST) and alanine aminotransferase (ALT), after the different treatments. ALT and AST were analyzed after treatment using the enzyme-linked immunosorbent assay (ELISA). The AST and ALT levels in the Fe@POS-DOX NP treatment group were lower than those in the free DOX injection group (Figures 5B and C). In this study, the Fe@POS-DOX NPs exhibited no appreciable in vivo systemic toxicity in animals. After treatment, the tumors and main organs were removed from the mice and stained with hematoxylin and eosin (H&E) for histopathological toxicity analysis. No anatomical changes were found, thus suggesting no obvious toxic effects on the major organs in the different treatment groups (Figure 5D). Terminal deoxynucleotidyl transferase (TdT)-mediated dUTP nick-end labeling (TUNEL) staining was performed to further detect the apoptosis of tumor cells in vivo.[28] The samples were incubated using a TUNEL apoptosis detection kit (Roche). The data revealed that more apoptotic cells with positive TUNEL staining were observed in the Fe@POS-DOX group than in the other groups (Figure 5E). The data revealed that Fe@POS-DOX efficiently promoted apoptosis in 4T1 breast cancer cells.

Conclusion

The novel monomer DOPA-NPC bearing unprotected phenolic hydroxyl groups was provided for controlled block copolymerization with Sar-NPC to synthesize POS. POS is an amphiphilic copolymer capable to form nanoparticles in

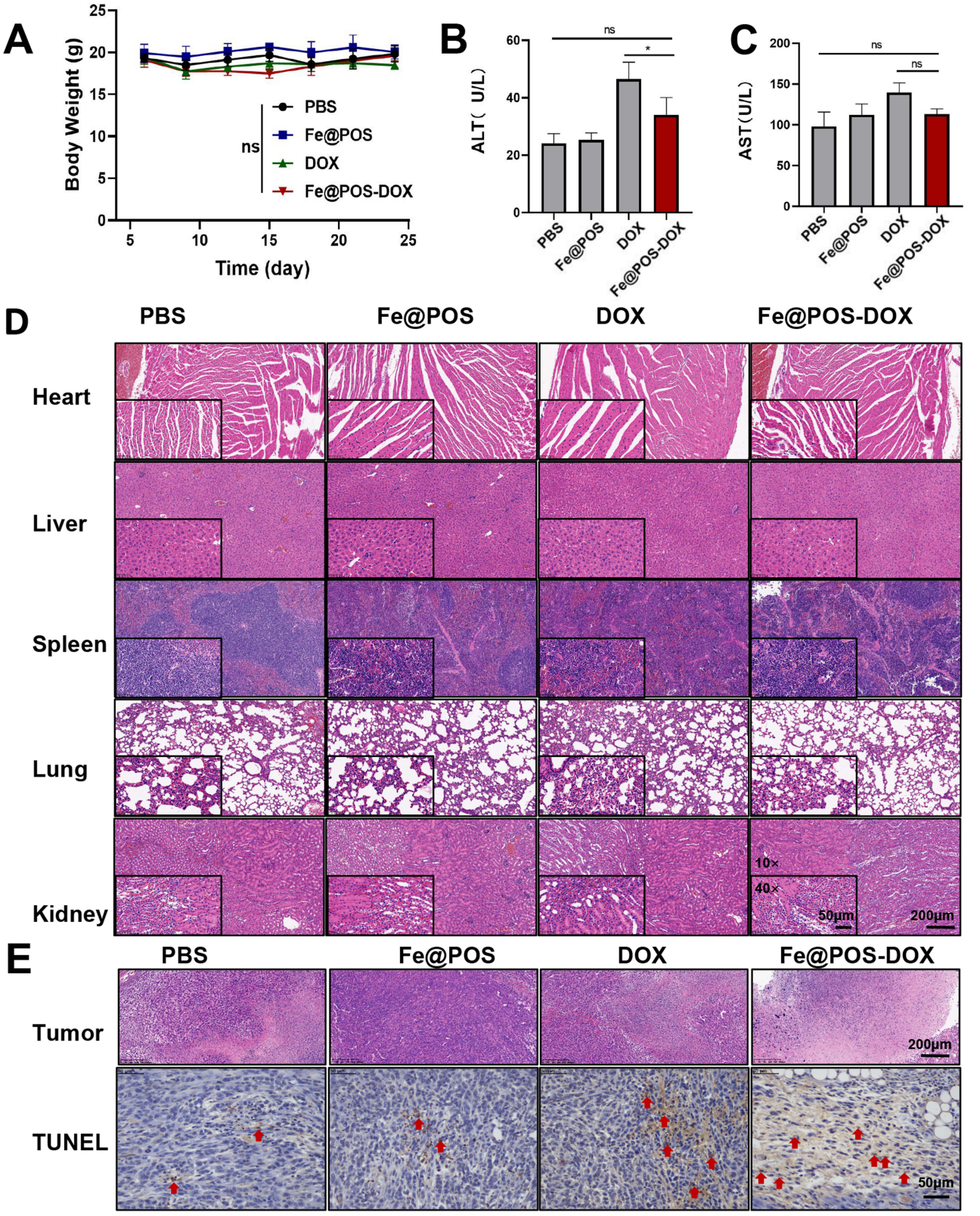

Figure 5 (**A**) The body weight of 4T1 tumor-bearing mice with different treatments. (**B** and **C**) Serum AST and ALT values in different treatment groups. (**D**) HE staining of the major organs in different treatment groups. (**E**) HE and TUNEL staining of tumors in different treatment groups.

water and encapsulate hydrophobic DOX, and the catechol groups of DOPA repeat units chelated Fe^{3+}. Fe@POS-DOX NPs that demonstrated high contrast efficiency (r_1 = 7.06 $mM^{-1}\cdot s^{-1}$) as T_1-weighted MRI contrast agents were developed with a retention time peak detected at 4 h after administration. Fe@POS-DOX NPs exhibited excellent tumor homing and low biotoxicity chemotherapy, and offered an improved tumor growth inhibition effect compared to that of free DOX at the same dose, thus displaying considerable potential for use in clinical applications.

Ethics Statement

All animal experiments were conducted with the approval of the Zhejiang University Experimental Animal Welfare Department (No. SRRSH20220903) and Ethics Committee under Institutional Animal Care and Use Committee guidelines.

Acknowledgments

The financial support was from National Natural Science Foundation of China (81871403, 81773096, 51822306), Major Program Co-sponsored by Province and Ministry (WKJ-ZJ-2210), Key Research and Development Program of Zhejiang Province (2019C03014), Ningbo Clinical Research Center for Medical Imaging (2021L003), the Project of NINGBO Leading Medical&Health Discipline(2022-S02).

Disclosure

The authors declare no conflicts of interest in this work.

References

1. He C, Liu D, Lin W. Nanomedicine Applications of Hybrid Nanomaterials Built from Metal–Ligand Coordination Bonds: nanoscale Metal–Organic Frameworks and Nanoscale Coordination Polymers. *Chem Rev*. 2015;115(19):11079–11108. doi:10.1021/acs.chemrev.5b00125
2. Shi J, Kantoff PW, Wooster R, et al. Cancer nanomedicine: progress, challenges and opportunities. *Nat Rev Cancer*. 2017;17:20–37.
3. Meel RVD, Sulheim E, Shi Y, et al. Smart cancer nanomedicine. *Nat Nanotechnol*. 2019;14(11):1007–1017.
4. Wang F, Wang YC, Dou S, et al. Doxorubicin-tethered responsive gold nanoparticles facilitate intracellular drug delivery for overcoming multidrug resistance in cancer cells. *ACS Nano*. 2011;5(5):3679–3692.
5. Park N, Wei C, Lai F, et al. Addressing drug resistance in cancer with macromolecular chemotherapeutic agents. *J Am Chem Soc*. 2018;140 (12):4244–4252.
6. Holohan C, Schaeybroeck SV, Longley DB, et al. Cancer drug resistance: an evolving paradigm. *Nat Rev Cancer*. 2013;13(10):714–726.
7. Wang J, Mao W, Lock LL, et al. The Role of Micelle Size in Tumor Accumulation, Penetration, and Treatment. *ACS Nano*. 2015;9(7):7195–7206.
8. Blanco E, Shen H, Ferrari M. Principles of nanoparticle design for overcoming biological barriers to drug delivery. *Nat Biotechnol*. 2015;33(9):941.
9. Ding Y, Xu H, Xu C, et al. A Nanomedicine Fabricated from Gold Nanoparticles-decorated Metal-Organic Framework for Cascade Chemo/ Chemodynamic Cancer Therapy. *Adv Sci*. 2020;7:2001060.
10. Li L, Fu S, Chen C, et al. Microenvironment-Driven Bioelimination of Magnetoplasmonic Nanoassemblies and Their Multimodal Imaging-Guided Tumor Photothermal Therapy. *ACS Nano*. 2016;10(7):7094–7105.
11. Shen S, Jiang D, Cheng L, et al. Renal-Clearable Ultra-Small Coordination Polymer Nanodots for Chelator-Free 64Cu-Labeling and Imaging-Guided Enhanced Radiotherapy of Cancer. *ACS Nano*. 2017;11(9):9103–9111.
12. Wang W, Liu X, Zheng X, et al. Biomineralization: an Opportunity and Challenge of Nanoparticle Drug Delivery Systems for Cancer Therapy. *Adv Healthcare Mater*. 2020;9(22):e2001117.
13. Zhou P, Li Z, Lu Y, et al. Telechelic Triblock Poly (α-Amino Acid)-Poly (Tetrahydrofuran)-Poly (α-Amino Acid) Copolymers: chain-End Transformation, Polymerization and pH-Responsive Hydrolysis. *Chine J Chem*. 2021;39(10):2852–2856.
14. Zhao L, Li N, Wang K, et al. A review of polypeptide-based polymersomes. *Biomaterials*. 2014;35(4):1284–1301.
15. Knight AS, Zhou EY, Francis MB, et al. Sequence programmable peptoid polymers for diverse materials applications. *Adv Mater*. 2015;27 (38):5665–5691.
16. Lu YZ, Gu AQ, Shen TL, et al. Clickable, Oxidation-Responsive and Enzyme-Degradable Polypeptide: synthesis, Characterization and Side Chain Modification. *Chine J Polymer Sci*. 2022. doi:10.1007/s10118-022-2745-x
17. Zhou P, Dai XG, Kong J, et al. Synthesis of Well-defined Poly(tetrahydrofuran)-b-Poly(a-amino acid)s via Cationic Ring-opening Polymerization (ROP) of Tetrahydrofuran and Nucleophilic ROP of N-thiocarboxyanhydrides. *Chine J Polymer Sci*. 2021;39(6):702–708.
18. Birke A, Ling J, Barz M. Polysarcosine-containing copolymers: synthesis, characterization, self-assembly, and applications. *Prog Polym Sci*. 2018;81:163.
19. Miao Y, Xie F, Cen J, et al. Fe $^{3+}$ @polyDOPA- *b* -polysarcosine, a T1-Weighted MRI Contrast Agent via Controlled NTA Polymerization. *ACS Macro Lett*. 2018;7(6):693–698.
20. Bakewell SJ, Carie A, Costich TL, et al. Imaging the delivery of drug-loaded, iron-stabilized micelles. *Nanomedicine*. 2017;13(4):1353–1362.
21. Thunus L, Lejeune R. Overview of transition metal and lanthanide complexes as diagnostic tools. *Coord Chem Rev*. 1999;28(184):125–155.
22. Smith BR, Gambhir SS. Nanomaterials for In Vivo Imaging. *Chem Rev*. 2017;117(3):901–986.
23. Dai Y, Xu C, Sun X, et al. Nanoparticle design strategies for enhanced anticancer therapy by exploiting the tumour microenvironment. *Chem Soc Rev*. 2017;46(12):3830–3852.

24. Liu Q, Lu X, Li L, et al. Probing the Reversible Fe^{3+}-DOPA-Mediated Bridging Interaction in Mussel Foot Protein-1. *J Phys Chem C*. 2016;120(38):21670–21677.
25. Zhou Z, Wang L, Chi X, et al. Engineered iron-oxide-based nanoparticles as enhanced T1 contrast agents for efficient tumor imaging. *ACS Nano*. 2013;7(4):3287–3296.
26. Feng Y, Zong Y, Ke T, et al. Pharmacokinetics, Biodistribution and Contrast Enhanced MR Blood Pool Imaging of Gd-DTPA Cystine Copolymers and Gd-DTPA Cystine Diethyl Ester Copolymers in a Rat Model. *Pharm Res*. 2006;23(8):1736–1742.
27. Maeda H, Nakamura H, Fang J. The EPR effect for macromolecular drug delivery to solid tumors: improvement of tumor uptake, lowering of systemic toxicity, and distinct tumor imaging in vivo. *Adv Drug Deliv Rev*. 2013;65(1):71–79.
28. Beckerman P, Bi-Karchin J, Park ASD, et al. Transgenic expression of human APOL1 risk variants in podocytes induces kidney disease in mice. *Nat Med*. 2017;23(4):429–438.